Journal of Power Sources 221 (2013) 300–307

Contents lists available at SciVerse ScienceDirect

Journal of Power Sources

journal homepage: www.elsevier.com/locate/jpowsour

Synthesis and electrochemical performance of $Li_{1.131}Mn_{0.504}Ni_{0.243}Co_{0.122}O_2$ cathode materials for lithium ion batteries via freeze drying

S.J. Shi, J.P. Tu*, Y.Y. Tang, Y.X. Yu, Y.Q. Zhang, X.L. Wang

State Key Laboratory of Silicon Materials, State Key Laboratory of Silicon Materials, Key Laboratory of Advanced Materials and Applications for Batteries of Zhejiang Province and Department of Materials Science and Engineering, Zhejiang University, Hangzhou 310027, China

HIGHLIGHTS

- Novel $Li_{1.131}Mn_{0.504}Ni_{0.243}Co_{0.122}O_2$ cathode material is synthesized by freeze drying.
- Initial discharge capacity of 246.5 mAh g^{-1} is obtained at 0.1 C (1 C = 200 mA g^{-1}).
- Initial discharge capacity of 197.8 mAh g^{-1} is obtained at 1 C
- Diffusion coefficients of Li^+ of 10^{-14}–10^{-18} cm^2 s^{-1} are obtained by GITT.

ARTICLE INFO

Article history:
Received 23 April 2012
Received in revised form
14 July 2012
Accepted 13 August 2012
Available online 21 August 2012

Keywords:
Lithium-rich layered oxide
Cathode
Freeze drying
Diffusion coefficient
Lithium ion battery

ABSTRACT

Well-formed $Li_{1.131}Mn_{0.504}Ni_{0.243}Co_{0.122}O_2$ cathode materials are synthesized via freeze drying followed by a solid state reaction at temperatures of 750–900 °C. Among these oxides, the one synthesized at 800 °C delivers the highest initial discharge capacity of 246.5 mAh g^{-1} at 0.1 C (1 C = 200 mA g^{-1}) between 2.5 V and 4.8 V. Enhancing the discharge rate to 1 C, initial capacity of 197.8 mAh g^{-1} is obtained, and 78.8% capacity is retained after 50 cycles. Furthermore, the diffusion coefficients of Li^+ in the lithium-rich layered oxide are about 10^{-14} cm^2 s^{-1} and 10^{-15} cm^2 s^{-1} for the initial charge platform at 3.90 V and 4.55 V, respectively, determined by galvanostatic intermittent titration technique (GITT). The $Li_{1.131}Mn_{0.504}Ni_{0.243}Co_{0.122}O_2$ prepared by freeze drying is a promising cathode material for lithium ion batteries.

1. Introduction

A number of efforts have been made recently to explore an alternative cathode material for lithium ion batteries with the performances superior to commercial $LiCoO_2$ [1–6]. Layered $LiMn_xNi_xCo_{1-2x}O_2$ ($0 \le x \le 0.5$), which exhibit excellent performances comparable to $LiCoO_2$ with respect to capacity, cycle stability, economy and safety have been extensively investigated [7–10]. $LiMn_{0.4}Ni_{0.4}Co_{0.2}O_2$, as one of the family members, possesses good electrochemical performances [11,12]. In order to meet exponential growth demands in portable electronics, and pure electric vehicle, excess lithium and manganese were added to form a Li-rich compound as $x\ Li_2MnO_3\cdot(1-x)\ LiMn_{0.4}Ni_{0.4}Co_{0.2}O_2$ ($0 < x < 1$). It was reported that the discharge capacity increased with the increase of x [13], and $0.4Li_2MnO_3\cdot0.6LiMn_{0.4}Ni_{0.4}Co_{0.2}O_2$ synthesized by Jin-Long Liu et al. delivered a discharge capacity of 250 mAh g^{-1} in the voltage range of 2–4.8 V [14]. The $x\ Li_2MnO_3\cdot(1-x)\ LiMn_{0.4}Ni_{0.4}Co_{0.2}O_2$ ($0 < x < 1$) are promising cathode materials for lithium ion batteries [15].

In addition, $xLi_2MnO_3\cdot(1-x)\ LiMO_2$ (M = Mn, Ni, Co) cathode materials are generally prepared by co-precipitation [16–19]. $Li[Li_{0.2}Mn_{0.54}Ni_{0.13}Co_{0.13}]O_2$ prepared by Yu et al. [20] was composed of spherical particles with sizes of 5–10 μm and exhibited good electrochemical performances. However, such slow co-precipitation method needs precise control of the reaction conditions. For example, the feeding speed should be adjusted every time to maintain the pH value. For these reasons, other method should also be investigated to synthesize the Li-rich layered compounds.

Freeze-drying method was ever used to synthesize cathode materials, such as $LiFePO_4$ [21–23], $LiMn_2O_4$ [24], $LiMO_2$ (M = Mn, Ni, Co) [25,26], and so on. Through simple freeze and sublimation processes, the uniform state in solution could be retained to obtain

* Corresponding author. Tel.: +86 571 87952856; fax: +86 571 87952573.
E-mail addresses: tujp@zju.edu.cn, tujplab@zju.edu.cn (J.P. Tu).

0378-7753/$ – see front matter © 2012 Elsevier B.V. All rights reserved.
http://dx.doi.org/10.1016/j.jpowsour.2012.08.031

the precursors which were mixed at atomic level. The preparation process is much simpler than co-precipitation and excellent electrochemical performances can also be obtained. In this present work, freeze-drying method is performed to synthesize a novel Li-rich compound $Li_{1.131}Mn_{0.504}Ni_{0.243}Co_{0.122}O_2$ ($0.3Li_2MnO_3 \cdot 0.7 LiMn_{0.4}Ni_{0.4}Co_{0.2}O_2$). The morphology, structure and electrochemical performances are studied in detail. The results show that the freeze-drying method should also be a promising way to prepare the Li-rich layered oxide cathode materials.

2. Experimental

In the freeze-drying method, stoichiometric amounts of $LiNO_3$, $Ni(NO_3)_2 \cdot 6H_2O$, $Co(NO_3)_2 \cdot 4H_2O$, and 50 wt.% $Mn(NO_3)_2$ solution were dissolved in the deionized water. Then a desired amount of urea was added in the solution. The molar ratio of urea and total transition metal ions (including Mn^{2+}, Ni^{2+} and Co^{2+}) was 1:3. Ammonia was used to adjust the pH value of the solution to 7.0. At last, 2 M citric acid solution was dropped into the mixture until a clear solution was obtained. The as-confected solution was cooled to −20 °C and freeze-dried at this temperature for more than 2 days until the mixture became dry. After that, the obtained powder was first calcined at 500 °C in air for 10 h to remove the organic compounds. Then the powder was ground thoroughly, and again calcined at 750 °C, 800 °C, 850 °C and 900 °C in air for 12 h. The as-synthesized oxides were named as LMNCO-750, LMNCO-800, LMNCO-850 and LMNCO-900 for short.

The morphologies and structures of the as-synthesized powders were characterized using field emission scanning electron microscopy (FESEM, S-4800 coupled with EDX), X-ray diffraction (XRD, RIGAKU D/Max-2550 with Cu Kα radiation). The element amount was analyzed by inductively coupled plasma emission spectrometer (ICP, IRIS Intrepid II).

The working electrodes were prepared by a slurry coating procedure. The slurry consisted of 85 wt.% as-synthesized materials, 10 wt.% carbon conductive agent (acetylene black) and 5 wt.% polyvinylidene fluoride (PVDF) was coated on aluminum foil. After dried at 90 °C for 24 h in vacuum, the sample was pressed under a pressure of 20 MPa. A metallic lithium foil served as the anode, 1 M $LiPF_6$ in ethylene carbonate (EC)-dimethyl carbonate (DMC) (1:1 in volume) was used as the electrolyte, and a polypropylene micro-porous film (Cellgard 2300) as the separator. The cells were assembled in an argon-filled glove box. The galvanostatic discharge–charge tests were performed with coin-type cells (CR2025) on a LAND battery program-control test system (Wuhan, China) between 2.5 and 4.8 V at the charge–discharge rates from 0.1 to 10 C (1 C = 200 mA g^{-1}) at room temperature. Galvanostatic intermittent titration technique (GITT) was also conducted on this apparatus in the voltage range of 2.5–4.8 V. Cyclic voltammetry (CV) test was carried out on an electrochemical workstation (CHI660C) in the potential window of 2.5–4.8 V (vs. Li/Li^+) at a scan rate of 0.1 mV s^{-1}. Electrochemical impedance spectroscopy (EIS) measurements were performed on this apparatus using a three-electrode cell with the layered oxide as the working electrode, metallic lithium foil as both the counter and reference electrodes. The amplitude of the AC signal was 5 mV over a frequency range from 100 kHz to 10 mHz at a charge state of 4.5 V.

3. Results and discussion

3.1. Material characterization

In order to remove the influence of the Li amount, chemical analysis of the element amount was performed by ICP. And the analytical results are shown in Table 1. The experimental Li ratio is found to be a little larger than the theoretical composition (Li = 1.131). However, the excess Li (3%) is almost consumed during the solid state reaction. Fig. 1 shows the XRD patterns of Li-rich oxides synthesized at different temperatures. For LMNCO-750, LMNCO-800 and LMNCO-850, the other peaks except the superlattice peaks between 20° and 25° can be indexed to α-$NaFeO_2$ structure with space group R-3m (Fig. 1(a)). The weak peaks between 20° and 25°, as clearly shown in Fig. 1(b), are consistent with the $LiMn_6$ cation arrangement that occurs in the transition metal layers of Li_2MnO_3 regions (nano-domains of Li_2MnO_3: It indicates that the Li_2MnO_3 regions are extremely small and they are distributed randomly throughout the composite structure [13]). These can be indexed to the monoclinic unit cell C2/m [27,28]. No peak for any impurity phase is detected in the patterns, indicating

Table 1
Results of ICP and the value of I_{003}/I_{104}, $(I_{006}+I_{012})/I_{101}$ calculated from the XRD data. The amount of Co is fixed as the theoretical value of 0.122.

Sample	Li	Mn	Ni	Co	I_{003}/I_{104}	$(I_{006}+I_{012})/I_{101}$
750 °C	1.13(8)	0.503(8)	0.242(6)	0.122	1.894	0.368
800 °C	1.13(6)	0.504(2)	0.242(8)	0.122	1.838	0.326
850 °C	1.13(6)	0.504(8)	0.242(8)	0.122	1.872	0.330
900 °C	1.13(2)	0.503(1)	0.243(1)	0.122		

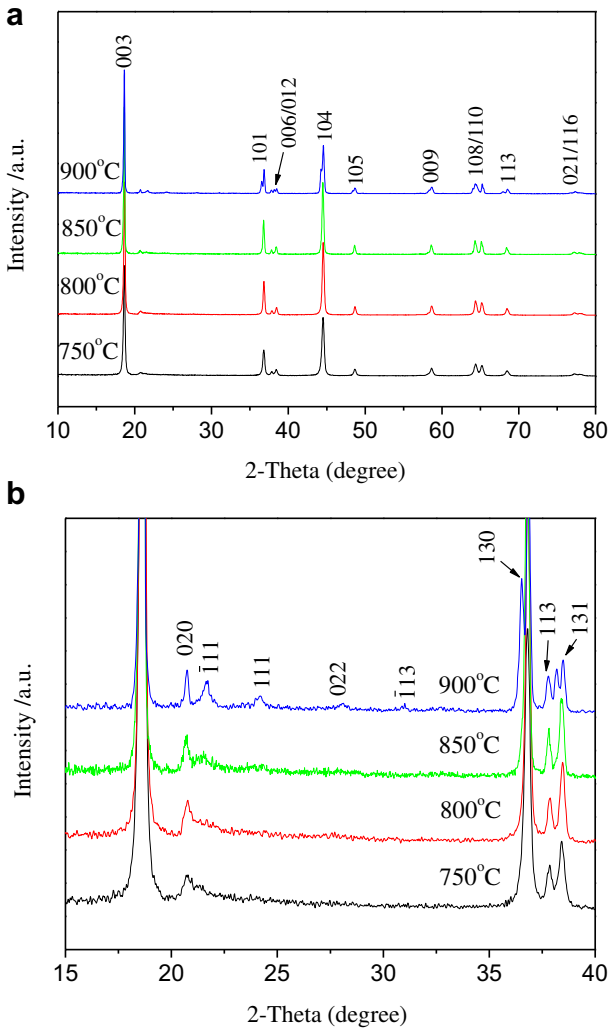

Fig. 1. XRD patterns of (a) $Li_{1.131}Mn_{0.504}Ni_{0.243}Co_{0.122}O_2$ synthesized at different temperatures, (b) A section of (a) from 15° to 40°.

the high purity of the as-synthesized oxides. However, for LMNCO-900, the peaks which belong to the monoclinic unit cell C2/m are not covered by the strong peaks of α-$NaFeO_2$ structure. The movement of the peaks indicates that an independent Li_2MnO_3 phase or large enough Li_2MnO_3 regions appear in the compound. It has been reported [13,29] that during the formation of the layered oxides, $LiMn_6$ cation arrangement has a priority to form first due to the thermodynamics factors. Therefore, such phenomenon results from the exorbitant high temperature performed during the solid state reaction. It will accelerate the formation of Li_2MnO_3 regions, and thus the superlattice between R-3m symmetry and C2/m symmetry is not well formed. In addition, as the synthesis temperature increases, the weak peaks with respect to the $LiMn_6$ cation arrangement between 20° and 25° become more symmetrical and sharper. The single broad peak at 20.9° of the oxides synthesized at lower temperature can be ascribed to an increase in the amount of stacking faults (shifting of the transition metal layers perpendicular to the layered (001) direction) [30]. The role of stacking faults on the electrochemical performances of the cathode material is unclear. However, from thermodynamics, the introduction of stacking faults and other defects may increase the energy state of the material, which may decrease the activation barrier for Li^+ diffusion and allow Li^+ to extract at a lower potential. Apparently, it will make the activation of the Li_2MnO_3 regions easier during charge process to some degree [30].

Furthermore, it has been reported that the ordering of the material structure can be indicated from the XRD patterns with the I_{003}/I_{104} and $(I_{006} + I_{012})/I_{101}$ (R factor) intensity ratios and the degree of (006)/(102) and (108)/(110) peak splitting [6,31,32]. The values of I_{003}/I_{104}, $(I_{006} + I_{012})/I_{101}$ of the compounds are shown in Table 1. All the oxides except LMNCO-900 have large ratios of I_{003}/I_{104} above 1.8 and small values of R factor below 0.4, indicating a well-formed layered structure. Among them, LMNCO-800 with distinct splitting (006)/(102) and (108)/(110) peak, and the smallest value of R factor will probably exhibit the best electrochemical performances.

The SEM images of the precursor and Li-rich oxides synthesized at different temperatures are shown in Fig. 2. As shown in Fig. 2(a), the precursor is similar to colloidal agglomerate with small particles uniformly dispersing on the surface. After solid state reaction, the organic components are removed and clear grain is obtained. Fig. 2(b)–(e) shows the morphologies of $Li_{1.131}Mn_{0.504}Ni_{0.243}Co_{0.122}O_2$ synthesized at different temperatures. Apparently, as the synthesis temperature increases, the particle size increases, too, and the crystallinity of the oxides becomes better. All the oxide particles are well-distributed, and the particle sizes are 50–100 nm,

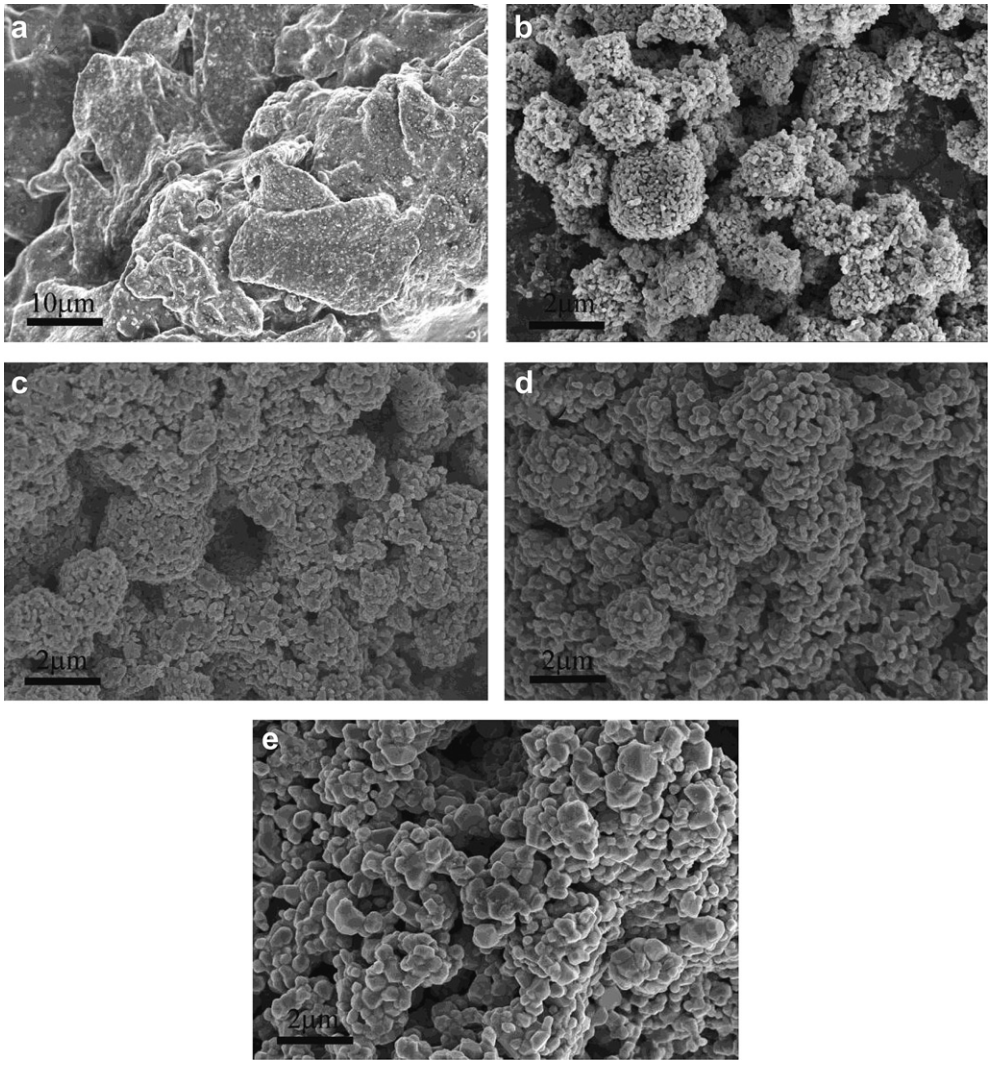

Fig. 2. SEM images of (a) precursor and $Li_{1.131}Mn_{0.504}Ni_{0.243}Co_{0.122}O_2$ synthesized at (b) 750 °C, (c) 800 °C, (d) 850 °C and (e) 900 °C.

100–200 nm, 200–300 nm and 200–500 nm for the ones synthesized at 750 °C, 800 °C 850 °C and 900 °C, respectively. The well-distributed particles are attributed to the homogenous precursor prepared by freeze drying. In addition, micron holes form due to the gas removal resulting from the oxidation of the organic components and nitrate. Furthermore, the second particles have the trend of forming balls due to the surface force. Such morphology is beneficial for reducing the agglomerate and available for the contact between the oxide particles and electrolyte.

3.2. Electrochemical properties

The initial charge–discharge curves of $Li_{1.131}Mn_{0.504}Ni_{0.243}Co_{0.122}O_2$ at 0.1 C (1 C = 200 mA g^{-1}) between 2.5 V and 4.8 V are shown in Fig. 3. As normal Li-rich layered oxides, there is a charge platform at about 4.5 V which appears only at the initial cycle. Among these oxides, LMNCO-800 has the largest initial charge and discharge capacity of 324.1 mAh g^{-1} and 246.5 mAh g^{-1}, respectively. The charge capacity approaches to its theoretical value (329 mAh g^{-1}). However, the initial charge–discharge efficiency is low, only about 76.1%. It has been reported [13,33] that the lost reversible capacity results from the removal of Li_2O in the Li_2MnO_3 regions. It is interesting that the electrochemical inactive Li_2MnO_3 region becomes active after removing of Li_2O from the lattice. This activation usually happens when the cell is charged above 4.4 V (vs. Li^+/Li), as the charge platform at about 4.5 V is observed in Fig. 3. LMNCO-750 and LMNCO-850 also have high charge and discharge capacity of 318 mAh g^{-1} and 237.4 mAh g^{-1}, 312.3 mAh g^{-1} and 235.1 mAh g^{-1}, respectively. However, LMNCO-900 without well-formed layered structure, exhibits the lowest charge and discharge capacity of only 277.9 mAh g^{-1} and 177.4 mAh g^{-1}, respectively. It is reported that Li_2MnO_3 synthesized at high temperature above 900 °C has rather poor electrochemical performance, unless it is well composed of R-3m symmetry structure to form superlattice [13,30,34]. Furthermore, the large particle sizes of LMNCO-900, as shown in Fig. 2(e), will partly lead to the poor electrochemical performance due to small specific surface area, long diffusion distance and so on. Because of the poor electrochemical performance of LMNCO-900, its cycle performance and rate capability are not displayed later.

Fig. 4 shows the cycle performance of $Li_{1.131}Mn_{0.504}Ni_{0.243}Co_{0.122}O_2$ at 1 C after 4 cycles at 0.1 C for activation. LMNCO-800 still has the highest initial discharge capacity of 197.8 mAh g^{-1} at 1 C. Such high discharge capacity at the evaluated rate is due to the well-formed structure and uniform particle size. After 50 cycles,

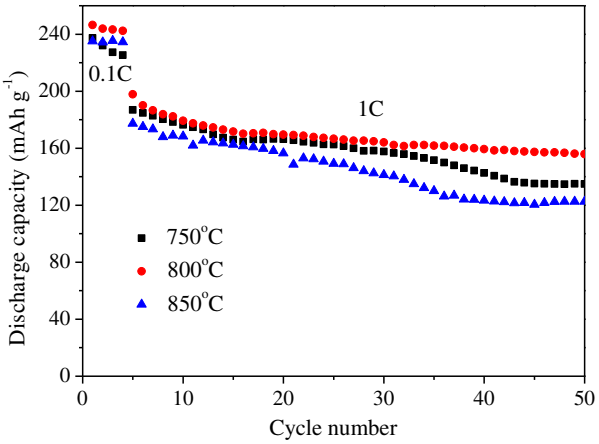

Fig. 4. Cycle performance of $Li_{1.131}Mn_{0.504}Ni_{0.243}Co_{0.122}O_2$ synthesized at different temperatures between 2.5 V and 4.8 V at 1 C.

about 20–30% discharge capacity is lost, and LMNCO-800 has the highest capacity retention of 78.8% at 1 C. The dissolution of the metal ions [35–38], especially the manganese ions during charge–discharge process has been demonstrated to mainly affect the cycle stability. The mechanism of the Mn dissolution can be explained as follows:

$$Mn^{3+} \xrightarrow{\text{charge–discharge}} Mn^{4+} + Mn^{2+} \quad (1)$$

The lower the synthesis temperature is, the lower the oxidation state of Mn is. Not all the Mn is in the oxidation state of 4^+, part will stay at the oxidation state of 3^+, and this part of Mn will be easily dissolved. In addition, during discharging to a low potential, part of Mn^{4+} will be reduced to Mn^{3+}. Furthermore, it is demonstrated that extensive removal of Li_2O appears to damage the electrode surface during electrochemical activation, leading to the increase of cell impedance [13,39]. And the destruction of the electrode surface will also accelerate the dissolution of the metal ions. So the discharge capacity decreases steadily on cycling, particularly when the high current rates are performed. The way of improving the cycle performance of Li-rich layered oxides has been extensively investigated [19,40]. Further work will also be carried out in our group.

The rate capability of $Li_{1.131}Mn_{0.504}Ni_{0.243}Co_{0.122}O_2$ is displayed in Fig. 5 from 0.1 C to 10 C between 2.5 V and 4.8 V. The cells are

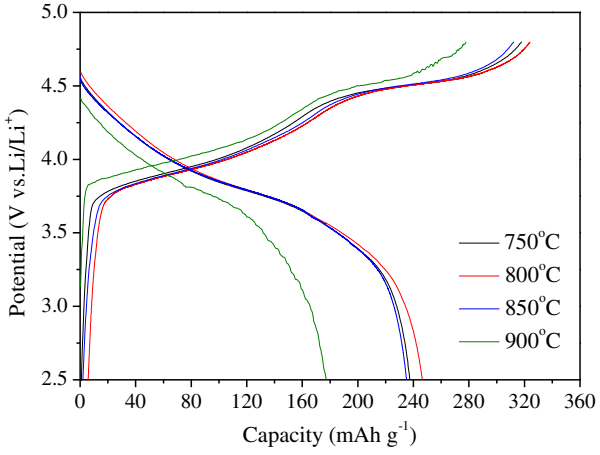

Fig. 3. Initial charge–discharge curves of $Li_{1.131}Mn_{0.504}Ni_{0.243}Co_{0.122}O_2$ synthesized at different temperatures.

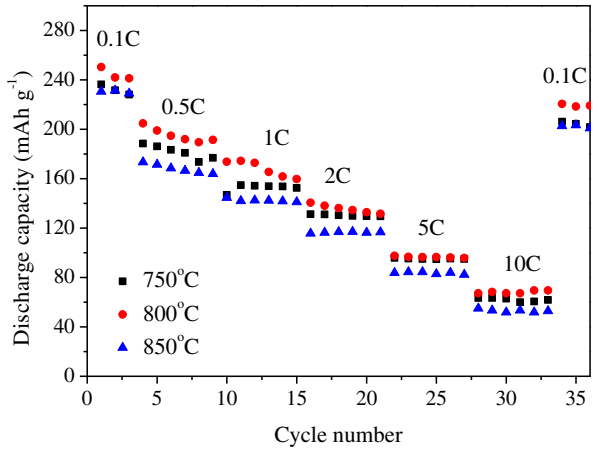

Fig. 5. Rate capability of $Li_{1.131}Mn_{0.504}Ni_{0.243}Co_{0.122}O_2$ synthesized at different temperatures in the voltage range of 2.5–4.8 V.

charged and discharged at the same rate. As shown in this figure, LMNCO-800 has the best rate capability. And the discharge capacity of 246.5, 204.8, 174.4, 140.5, 97.5 and 69.4 mAh g^{-1} are obtained at 0.1 C, 0.5 C, 1 C, 2 C, 5 C and 10 C, respectively. The decrease of the capacity at elevated rate is ascribed to the abundant lattice disorders produced during the transformation from $Li_{1.131}Mn_{0.504}Ni_{0.243}Co_{0.122}O_2$ to $Li_xMn_{0.504}Ni_{0.243}Co_{0.122}O_2$ as the Li_2O is removed [41]. They will block the transfer of Li^+ and thus the diffusion coefficient of Li^+ decreases. This is accordant with the result of the GITT test later. While LMNCO-850 has the worst rate capability, which is due to the largest particles, smallest surface areas and the longest diffusion distance.

CV tests are performed to further understand the materials synthesized at different temperatures. Fig. 6(a) shows the initial CV curves of $Li_{1.131}Mn_{0.504}Ni_{0.243}Co_{0.122}O_2$. The curves are sharp, symmetrical and accordant with the initial charge–discharge curves. There are two main oxidation peaks, one at about 3.9 V and another at about 4.6 V. The peak at low potential is ascribed to the extraction of Li^+ from the $LiMO_2$ (M = Mn, Ni, Co) structure, which is accompanying with oxidation of Ni^{2+}. And another peak at 4.6 V is related to the activation of the Li_2MnO_3 regions. It has been demonstrated that when the Li-rich oxide is charged above 4.4 V, excess Li would extract from the Li_2MnO_3 region, accompanying with loss of O [33]. Interestingly, the inactive Li_2MnO_3 becomes active [MnO_2], and during the following discharge process, a high initial discharge capacity of 246.5 mAh g^{-1} is obtained in our work, approaching to the theory capacity (~260 mAh g^{-1}, calculated from the mass of the parent $xLi_2MnO_3 \cdot (1-x)LiMO_2$ electrode before electrochemical activation when charged and discharged in the potential of 2–5 V (vs. Li/Li^+)). However, in the second cycle, the activation peak disappears, as shown in Fig. 6(b). Furthermore, it is clearly shown that the activation peak becomes weak, as the synthesis temperature increases. It is demonstrated [30] that the Li-rich layered oxide synthesized at lower temperature may possess more defects, such as stacking faults, dislocations and vacancy, which may decrease the activation barrier for Li^+ diffusion. Thus, it is easier for the activation of Li_2MnO_3 regions.

Fig. 7(a) shows the Nyquist plots of LMNCO-750, LMNCO-800 and LMNCO-850 at the charge state of 4.5 V in the third cycle. The shapes of the Nyquist plots are similar. They are composed of a small interrupt and a semicircle in the high frequency,

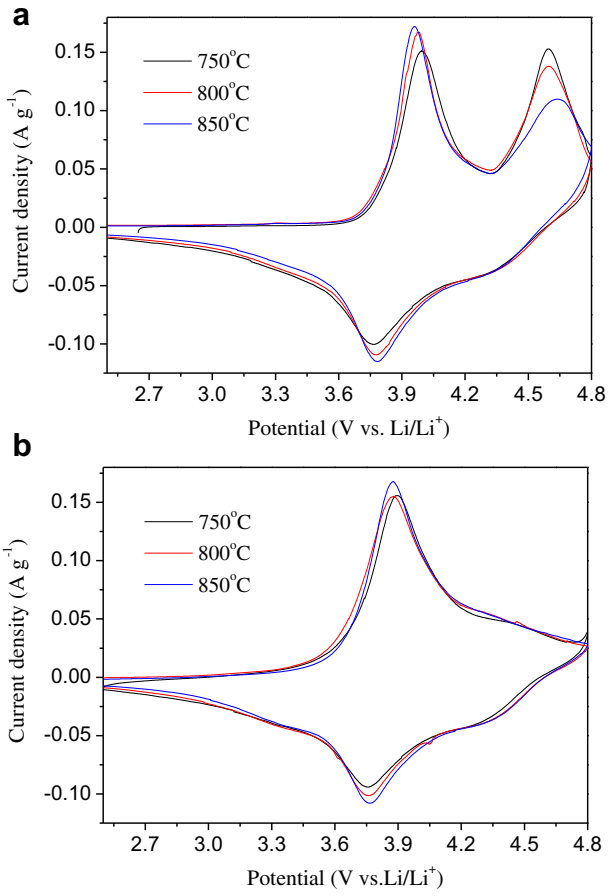

Fig. 6. CV curves of (a) $Li_{1.131}Mn_{0.504}Ni_{0.243}Co_{0.122}O_2$ synthesized at different temperatures in the initial cycle and (b) in the second cycle (scan rate: 0.1 mV s^{-1}, potential range: 2.5–4.8 V).

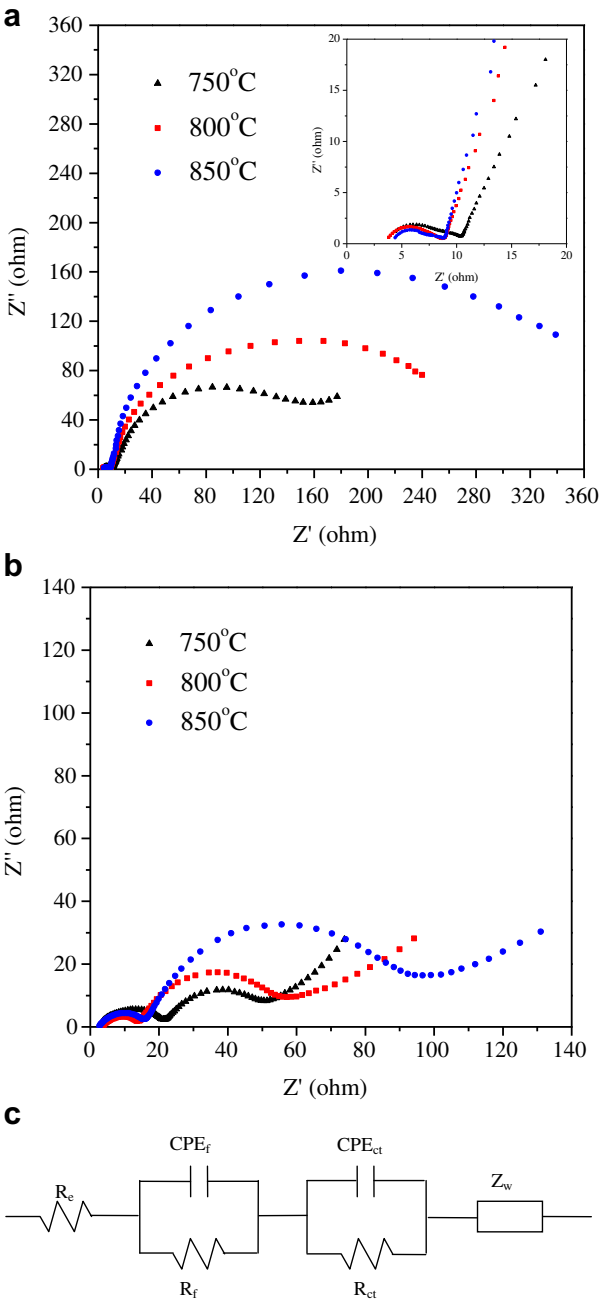

Fig. 7. Nyquist plots of (a) $Li_{1.131}Mn_{0.504}Ni_{0.243}Co_{0.122}O_2$ and (b) $LiMn_{0.4}Ni_{0.4}Co_{0.2}O_2$ synthesized at different temperatures in the third cycle at a charge state of 4.5 V, (c) equivalent circuit performed to fit the curves in (a) and (b).

a semicircle in the high to medium frequency and a quasi-straight line in the low frequency. The small interrupt in the high frequency is almost the same for all the oxide electrodes, which corresponds to the solution impedance R_e. The small semicircle in the high frequency is assigned to the impedance (R_f) of Li^+ diffusion in the surface layer (SEI film); another semicircle in the high to medium frequency is assigned to the impedance of charge transfer reaction (R_{ct}); and the quasi-straight line in the low frequency is assigned to Warburg impedance which refers to the impedance of Li^+ diffusion in bulk material [17,42]. For comparison, the Nyquist plots of $LiMn_{0.4}Ni_{0.4}Co_{0.2}O_2$ at the charge state of 4.5 V are shown in Fig. 7(b). It reveals distinctly that R_{ct} of Li_2MnO_3-based material is much larger than that of $LiMn_{0.4}Ni_{0.4}Co_{0.2}O_2$. The quasi-straight line in the low frequency which is assigned to Warburg impedance even becomes less evident or disappears due to so large R_{ct}. Such phenomenon can be ascribed to the poor conductivity of Li_2MnO_3 regions [13]. In order to further understand the Nyquist plots, an equivalent circuit is used to fit them, as shown in Fig. 7(c). CEP_f, CEP_{ct} and Z_w represent the non-ideal capacitance of the surface layer, non-ideal capacitance of the double-layer and Warburg impedance, respectively [17,43]. The values of R_f are calculated as 7.09 Ω, 5.32 Ω and 5.51 Ω for LMNCO-750, LMNCO-800 and LMNCO-850, respectively. There is no distinct difference for these oxides. However, the value of R_{ct} increases distinctly with the increase of synthesis temperature, 127.1 Ω, 234.7 Ω and 372.8 Ω for LMNCO-750, LMNCO-800 and LMNCO-850, respectively. Such phenomenon is similar to that observed by Zheng et al. [44] and in our previous work [45]. In addition, R_{ct} of the $LiMn_{0.4}Ni_{0.4}Co_{0.2}O_2$ also has the same rule, as shown in Fig. 7(b).

Because of the less evident Warburg region, the diffusion coefficient of Li^+ (D_{Li}^+) in the electrode cannot be calculated from the Warburg region in Nyquist plots. In view of this, GITT test was

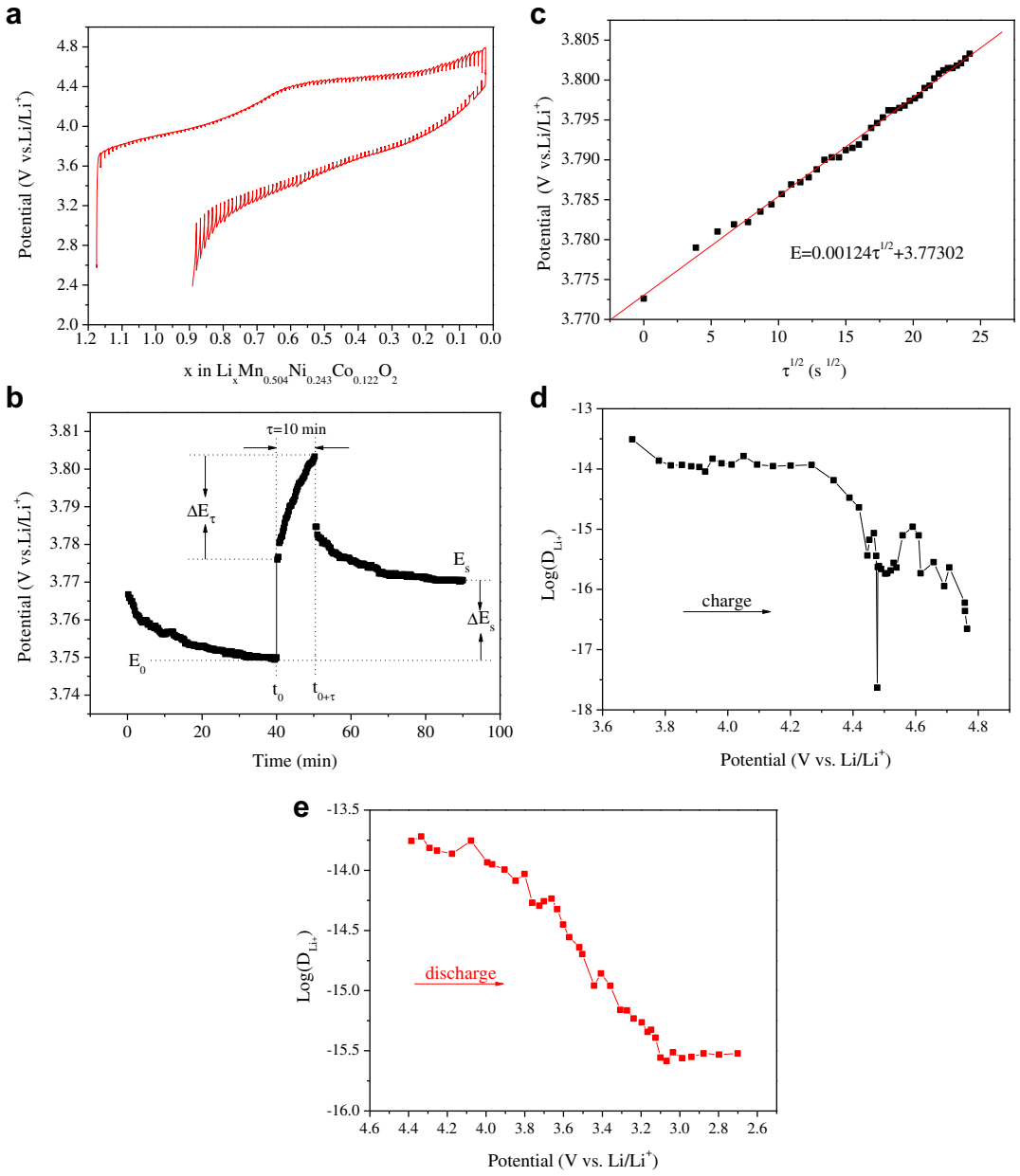

Fig. 8. (a) GITT curves of $Li_{1.131}Mn_{0.504}Ni_{0.243}Co_{0.122}O_2$ in the initial charge–discharge up to 4.8 V (current flux: 20 mA g^{-1}, time interval: 40 min), (b) t vs. E profile for a single GITT titration, (c) linear behavior of E vs. $\tau^{1/2}$, (d) diffusion coefficients of Li^+ in $Li_{1.131}Mn_{0.504}Ni_{0.243}Co_{0.122}O_2$ at different charge states, (e) diffusion coefficients of Li^+ at different discharge states.

carried out to evaluate D_{Li}^{+} in the Li_2MnO_3-based oxide. Fig. 8(a) shows the GITT curve of $Li_{1.131}Mn_{0.504}Ni_{0.243}Co_{0.122}O_2$ synthesized at 800 °C during the initial charge–discharge process between 2.5 V and 4.8 V. The chemical diffusion coefficient of Li^+ (D_{Li+}) is calculated according to Eq. (2) derived by Weppner and Huggins as follows [46]:

$$D_{Li^+} = \frac{4}{\pi}\left(\frac{mV_M}{MA}\right)^2\left(\frac{\Delta E_s}{\tau(dE_\tau/d\sqrt{\tau})}\right)^2\left(\frac{\tau \le L^2}{D_{Li^+}}\right) \quad (2)$$

where V_M is the molar volume of the compound, which is 20.31 $cm^3\ mol^{-1}$ deduced from the crystallographic data. M and m are the molecular weight and mass of the $Li_{1.131}Mn_{0.504}Ni_{0.243}Co_{0.122}O_2$, respectively. A is the interface between the active material and electrolyte, which is based on the result of the BET test (6.423 $m^2\ g^{-1}$). L is the radius of the active particle. Fig. 8(b) shows a typical t vs. E profile for a single titration. If E vs. $\tau^{1/2}$ shows a straight line behavior over the entire period of current flux, as shown in Fig. 8(c), Eq. (2) can be further simplified as [46]

$$D_{Li^+} = \frac{4}{\pi\tau}\left(\frac{mV_M}{MA}\right)^2\left(\frac{\Delta E_s}{\Delta E_\tau}\right)^2 \quad (3)$$

Based on Eq. (3) and GITT measurement, the diffusion coefficients of Li^+ at varied voltages can be obtained, as shown in Fig. 8(d) and (e). The results of the charge section have a similar rule to the initial charge curve shown in Fig. 3. At the charge process from 3.8 V to 4.3 V, the Li^+ probably extracts from the $LiMO_2$ (M = Mn, Ni, Co) regions. The D_{Li^+} is almost a constant, about $10^{-14}\ cm^2\ s^{-1}$ at that process. However, at the end of the first charge platform (from 4.25 V to 4.48 V), the D_{Li^+} decreases rapidly. The smallest D_{Li^+} of $5.853 \times 10^{-18}\ cm^2\ s^{-1}$ is obtained at 4.48 V. As the charge process goes along, the D_{Li^+} increases to about $10^{-15}\ cm^2\ s^{-1}$ at the charge platform of about 4.55 V, corresponding to the activation section of Li_2MnO_3 regions. It probably indicates that the diffusion of Li^+ in Li_2MnO_3 regions is slower than that in $LiMO_2$ (M = Mn, Ni, Co) regions. In comparison with typical layered oxides such as $LiCoO_2$ (10^{-7}–$10^{-11}\ cm^2\ s^{-1}$) [47] and $LiNi_{1/3}Co_{1/3}Mn_{1/3}O_2$ (10^{-9}–$10^{-10}\ cm^2\ s^{-1}$) [48], the D_{Li^+} obtained here is extremely small. It is attributed to the existence of Li_2MnO_3 regions which may be one of the significant factors for the unsatisfactory rate capability of Li-rich oxide cathode. Similarly, at the end of the charge, the D_{Li^+} decreases again.

Fig. 8(e) shows the variation of D_{Li^+} during the whole discharge process. It decreases almost linearly from the beginning to about 3.1 V, and becomes stable at the end of discharge. The D_{Li^+} obtained here is also extremely small comparing to the typical layered oxide. This is understandable because abundant Li^+ and O were removed during the transformation from $Li_{1.131}Mn_{0.504}Ni_{0.243}Co_{0.122}O_2$ to Li_xMO_2. So the resultant crystal lattice is not perfect, which therefore retards the diffusion of Li^+. Furthermore, the reactions during the charge–discharge process are extremely complex, which include not only Li^+ diffusion but also oxygen loss, metal ion dissolution and structural rearrangement. Thus, the D_{Li^+} obtained here should be regarded as pseudo or apparent diffusion coefficients [41].

4. Conclusions

$Li_{1.131}Mn_{0.504}Ni_{0.243}Co_{0.122}O_2$ cathode materials were synthesized via freeze drying followed by high-temperature solid state reaction. Well-formed structure can be obtained from 750 °C to 850 °C, and the oxide synthesized at 800 °C delivers the highest initial discharge capacity of 246.5 mAh g^{-1} at 0.1 C and 197.8 mAh g^{-1} at 1 C in the voltage range of 2.5–4.8 V. 78.8% capacity is retained after 50 cycles at 1 C. The decrease of the capacity results from the side reactions. Furthermore, small D_{Li^+} calculated by GITT indicates that the diffusion of Li^+ in the Li-rich layered oxide is slow due to the existence and transformation of Li_2MnO_3 regions. $Li_{1.131}Mn_{0.504}Ni_{0.243}Co_{0.122}O_2$ prepared by freeze drying will be a promising cathode material for lithium ion batteries.

Acknowledgments

This work is supported by Key Science and Technology Innovation Team of Zhejiang Province (2010R50013) and Fundamental Research Funds for the Central Universities (2011QNA4006).

References

[1] Z.H. Tang, Z.X. Wang, X.H. Li, W.J. Peng, J. Power Sources 204 (2012) 187.
[2] X.T. Chen, J.P. Tu, Y.Z. Yang, H.M. Wu, J.Y. Xiang, Phys. Scr. T129 (2007) 49.
[3] W.C. West, J. Soler, B.V. Ratnakumar, J. Power Sources 204 (2012) 200.
[4] Z.H. Tang, Z.X. Wang, X.H. Li, W.J. Peng, J. Power Sources 208 (2012) 237.
[5] H.M. Wu, J.P. Tu, Y.F. Yuan, J.Y. Xiang, X.T. Chen, X.B. Zhao, G.S. Cao, J. Electroanal. Chem. 608 (2007) 8.
[6] H.M. Wu, J.P. Tu, X.T. Chen, Y.F. Yuan, Y. Li, X.B. Zhao, G.S. Cao, J. Power Sources 159 (2006) 291.
[7] S.T. Myung, K.S. Lee, Y.K. Sun, H. Yashiro, J. Power Sources 196 (2011) 7039.
[8] C.M. Ban, Z. Li, Z.C. Wu, M.J. Kirkham, L. Chen, Y.S. Jung, E.A. Payzant, Y.F. Yan, M.S. Whittingham, A.C. Dillon, Adv. Energy Mater. 1 (2011) 58.
[9] S.J. Shi, J.P. Tu, Y.J. Mai, Y.Q. Zhang, C.D. Gu, X.L. Wang, Electrochim. Acta 63 (2012) 112.
[10] M.M. Ma, N.A. Chernov, B.H. Toby, P.Y. Zavalij, M.S. Whittingham, J. Power Sources 165 (2007) 517.
[11] H.S. Kim, K.T. Kim, P. Periasamy, Electronic Mater. Lett. 2 (2006) 119.
[12] J.K. Ngal, N.A. Chernov, M.M. Ma, M. Mamak, P.Y. Zavalij, M.S. Whittingham, J. Mater. Chem. 14 (2004) 214.
[13] M.M. Thackeray, S.H. Kang, C.S. Johnson, J.T. Vaughey, R. Benedek, S.A. Hackney, J. Mater. Chem. 17 (2007) 3053.
[14] L.J. Long, W. Jie, X.Y. Yao, Electrochim. Acta 56 (2011) 7392.
[15] J. Li, R. Klöpsch, M.C. Stan, S. Nowak, M. Kunze, M. Winter, S. Passerini, J. Power Sources 196 (2011) 4821.
[16] J. Gao, J. Kim, A. Manthiram, Electrochem. Commun. 11 (2009) 84.
[17] J. Liu, Q.Y. Wang, B.R. Jayan, A. Manthiram, Electrochem. Commun. 12 (2010) 750.
[18] J. Liu, B.R. Jayan, A. Manthiram, J. Phys. Chem. C 114 (2010) 9528.
[19] J.M. Zheng, Z.R. Zhang, X.B. Wu, Z.X. Dong, Z. Zhu, Y. Yang, J. Electrochem. Soc. 155 (2008) A775.
[20] D.Y.W. Yu, K. Yanagida, H. Nakamura, J. Electrochem. Soc. 157 (2010) A1177.
[21] X.L. Xi, G.L. Chen, Z.R. Nie, S. He, X. Pi, X.G. Zhu, J.J. Zhu, T.Y. Zuo, J. Alloys Compd. 497 (2010) 377.
[22] V. Palomares, A. Goni, I.G. Muroa, I. Meatza, M. Bengoechea, O. Miguel, T. Rojo, J. Power Sources 171 (2007) 879.
[23] E. Zhecheva, M. Mladenov, P. Zlatilova, V. Koleva, R. Stoyanov, J. Phys. Chem. Solids 71 (2010) 848.
[24] T.L. Mercier, J. Gaubicher, E. Bermejo, Y. Chabre, M. Quarton, J. Mater. Chem. 9 (1999) 567.
[25] O.A. Shlyakhtin, Y.S. Yoon, S.H. Choi, Y.J. Oh, Electrochim. Acta 50 (2004) 505.
[26] S.H. Choi, O.A. Shlyakhtin, J. Kim, Y.S. Yoon, J. Power Sources 140 (2005) 355.
[27] J.S. Kim, C.S. Johnson, J.T. Vaughey, M.M. Thackeray, S.A. Hackney, W. Yoon, C.P. Grey, Chem. Mater. 16 (2004) 1996.
[28] W.S. Yoon, S. Iannopollo, C.P. Grey, D. Carlier, J. Gorman, J. Reed, G. Ceder, Electrochem. Solid State Lett. 7 (2004) A167.
[29] N. Yabuuchi, K. Yoshii, S.T. Myung, I. Nakai, S. Komaba, J. Am. Chem. Soc. 133 (2011) 4404.
[30] D.Y.W. Yu, K. Yanagid, Y. Kato, H. Nakamur, J. Electrochem. Soc. 156 (2009) A417.
[31] C.X. Cheng, L. Tan, H.W. Liu, X.T. Huang, Mater. Res. Bull. 46 (2011) 2032.
[32] A.M.A. Hashem, A.E. Abdel-Ghany, A.E. Eid, J. Trottier, K. Zaghib, A. Mauger, C.M. Julien, J. Power Sources 196 (2011) 8632.
[33] C.S. Johnson, N. Li, C. Lefief, J.T. Vaughey, M.M. Thackeray, Chem. Mater. 20 (2008) 6095.
[34] A.D. Robertson, P.G. Bruce, Chem. Mater. 15 (2003) 1984.
[35] A. Ito, D. Li, Y. Sato, M. Arao, M. Watanabe, M. Hatano, H. Horie, Y. Ohsawa, J. Power Sources 195 (2010) 567.
[36] J. Park, J.H. Seo, G. Plett, W. Lu, A.M. Sastry, Electrochem. Solid-State Lett. 14 (2011) A14.
[37] D.H. Jang, Y.J. Shin, S.M. Oh, J. Electrochem. Soc. 143 (1996) 2204.
[38] M. Wohlfahrt-Mehrens, C. Vogler, J. Garche, J. Power Sources 127 (2004) 58.
[39] Z.Q. Deng, A. Manthiram, J. Phys. Chem. C 115 (2011) 7097.
[40] Y.S. Jung, A.S. Cavanagh, Y.F. Yan, S.M. George, A. Manthiram, J. Electrochem. Soc. 158 (2011) A1298.
[41] Z. Li, F. Du, X.F. Bie, J. Phys. Chem. C 114 (2010) 22751.

[42] S.K. Hu, G.H. Cheng, M.Y. Cheng, B.J. Hwang, R. Santhanam, J. Power Sources 188 (2009) 564.
[43] F. Wu, M. Wang, Y.F. Su, S. Chen, B. Xu, J. Power Sources 191 (2009) 628.
[44] J.M. Zheng, X.B. Wu, Y. Yang, Electrochim. Acta 56 (2011) 3071.
[45] S.J. Shi, Y.J. Mai, Y.Y. Tang, C.D. Gu, X.L. Wang, J.P. Tu, Electrochim. Acta 77 (2012) 39.
[46] W. Weppner, R.A. Huggins, J. Electrochem. Soc. 124 (1977) 1569.
[47] M. Park, X.C. Zhang, M. Chung, G.B. Less, A.M. Sastry, J. Power Sources 195 (2010) 7904.
[48] K.M. Shaju, G.V.S. Rao, B.V.R. Chowdariz, J. Electrochem. Soc. 151 (2004) A1324.